

Generating particle-like scattering states in wave transport

Stefan Rotter,* Philipp Ambichl, and Florian Libisch

Institute for Theoretical Physics, Vienna University of Technology, A-1040 Vienna, Austria, EU

(Dated: November 10, 2018)

We introduce a procedure to generate scattering states which display trajectory-like wave function patterns in wave transport through complex scatterers. These deterministic scattering states feature the dual property of being eigenstates to the Wigner-Smith time-delay matrix Q and to the transmission matrix $t^\dagger t$ with classical (noiseless) transmission eigenvalues close to 0 or 1. Our procedure to create such beam-like states is based solely on the scattering matrix and successfully tested numerically for regular, chaotic and disordered cavities. These results pave the way for the experimental realization of highly collimated wave fronts in transport through complex media with possible applications like secure and low-power communication.

PACS numbers: 05.60.-k,73.23.-b,42.25.-p,43.20.+g

The scattering of waves through complex systems is a central subject in physics occurring on a variety of length and time scales. Coherent electron transport through mesoscopic systems, light transmission through optical devices as well as all matters related to room acoustics are just a few examples of this kind. Recently, enormous experimental progress has been made in the ability to determine the system-specific scattering matrix of such complex systems either explicitly [1] or implicitly by methods like adaptive wave-front shaping [2] and optical phase conjugation [3]. These advances have led to spectacular results for complex scatterers which could be made transparent [2, 3] or put to use for focusing an incident wave on a spot size below the diffraction limit [4].

Common to all such applications is the aim to employ the information stored in the scattering matrix to create scattering states with specific properties. A very fundamental property a scattering state can have is to follow the particle-like bouncing pattern of a classical trajectory throughout the entire scattering process [5]. Such “classical” scattering states play a key role for the wave-to-particle crossover, for the emergence of geometrical optics out of physical optics and for the breakdown of universality in coherent transport [6–10]. However interesting these classical states may be, in complex scattering geometries they turn out to be as elusive as the proverbial needle in a haystack.

In this Letter we propose an operational procedure to generate such states explicitly. Our approach is illustrated with the example of a two-dimensional rectangular cavity through which waves can be scattered by two leads attached to the left and right (see Fig. 1). With each lead carrying N open modes the $(2N \times 2N)$ -dimensional unitary scattering matrix of this device has the form,

$$S = \begin{pmatrix} r & t' \\ t & r' \end{pmatrix}, \quad (1)$$

where each of the four blocks contains $N \times N$ complex elements for the energy dependent transmission (t) and reflection (r) amplitudes [(unprimed) primed amplitudes

designate injection from the (left) right lead]. The total transmission T through this resonant cavity is given as $T = \text{Tr}(t^\dagger t) = \sum_{n=1}^N \tau_n$, where the $\tau_n \in [0, 1]$ are the real transmission eigenvalues of the hermitian matrix $t^\dagger t$. Among the associated eigenstates $|\tau\rangle$ those with eigenvalues close to $\tau=0$ or $\tau=1$ are termed “noiseless states” as they feature a vanishing contribution to electronic shot noise [6–10]. Since all of the desired “classical” states with a trajectory-like bouncing pattern must have such deterministic values of transmission they are all part of a highly degenerate noiseless subspace associated with $\tau = 0, 1$. Consider in Fig. 1a,b two randomly chosen states with $\tau > 0.99$ from this subspace, calculated with the Modular Recursive Green’s Function Method [11].

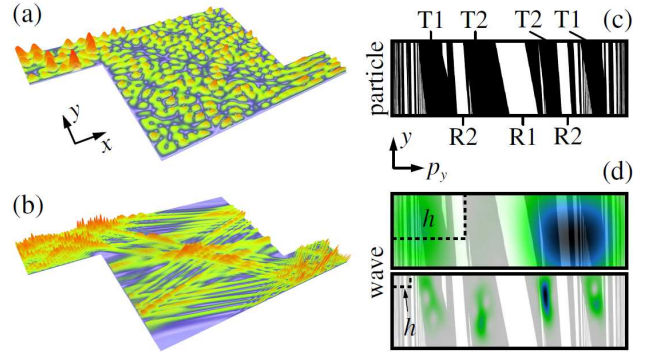


FIG. 1: (Color online) Scattering through a rectangular cavity (flux injected through the left lead of width d): (a),(b) Wave function densities of transmission eigenstates $|\tau\rangle$ of $t^\dagger t$ with similar transmission eigenvalues $\tau > 0.99$ but different wave numbers: (a) $k = 5.5\pi/d$, (b) $k = 75.5\pi/d$. (c) Classical surface of section, recorded for trajectories which enter at the left lead mouth with vertical position y and transverse momentum p_y . The largest of the transmission/reflection bands (black/white) are labeled by T1,T2/R1,R2 (bands which are equivalent in an extended zone scheme are given the same label). (d) Husimi distributions of the states shown in (a) (upper panel) and in (b) (lower panel). The size (area) of the Planck cell h is indicated by dashed black frames and the underlying classical phase space is shown in gray.

The first such state (see Fig. 1a) was calculated at a low wave number where only $N = 5$ lead modes are open. To understand the composition of classical trajectories contributing to this state we evaluate the Poincaré surface of section (PSS) at the entrance lead junction (see Fig. 1c). With transmitted (reflected) trajectories being shown in black (white) the PSS features a banded pattern with the individual bands being made up of bundles of trajectories which all have equivalent bouncing patterns [12]. The contributions of different phase space bands to the state $|\tau\rangle$ in Fig. 1a are revealed by comparing its quantum phase space distribution (Husimi function) $H(y, p_y) = |\langle \tau | y, p_y \rangle|^2$ with the PSS, where $|y, p_y\rangle$ is a minimum uncertainty state at y, p_y . The corresponding plot in Fig. 1d (upper panel) shows that the banded structure of the PSS is not resolved by this state—in line with the fact that the individual areas of the largest phase space bands are all smaller than the Planck constant h , i.e., the lower resolution limit in wave scattering. Rather, this state is composed of many interfering contributions from both transmitting *and* reflecting bands.

The situation is different when, for smaller wave lengths, the size of the Planck cell is well below the size of the largest phase space bands [6–10]. Consider, e.g., the noiseless transmission eigenstate $|\tau\rangle$ with $N = 75$ shown in Fig. 1b. We find that the Husimi distribution of this state [see Fig. 1d (lower panel)] is entirely located on transmission bands, indicating that full transmission is reached here by resolving the classical phase space. Since, however, more than one transmission band contribute (mostly T1 and T2) clear signatures of classical bouncing patterns are still absent in the corresponding scattering wave function (Fig. 1b). This is a result of the indiscriminate mixing of states in the degenerate noiseless subspace. This problem may be circumvented by explicitly constructing scattering states which lie on individual phase space bands [9]. In a real experiment such a protocol, however, meets the problem that the classical phase space structure is typically unknown for a complex scatterer. A viable measurement protocol which is based solely on experimentally accessible quantities like the scattering matrix [1] would thus be highly desirable.

To resolve the contributions of individual phase space bands we present an approach based on the observation that all trajectories in the same band have a characteristic and very similar cavity dwell time. In analogy to eikonal theory we may thus “label” contributions from different bands by their respective dwell times (or path lengths). In wave scattering the closest analogues to classical dwell times are the “proper delay times”, i.e., the eigenvalues of the Wigner-Smith time-delay matrix [13],

$$Q = i\hbar \frac{\partial S^\dagger}{\partial E} S = i\hbar \begin{pmatrix} \dot{r}^\dagger r + \dot{t}^\dagger t & \dot{r}^\dagger t' + \dot{t}^\dagger r' \\ \dot{t}^\dagger r + \dot{r}'^\dagger t & \dot{r}'^\dagger r' + \dot{t}'^\dagger t' \end{pmatrix}, \quad (2)$$

where the dots stand for the energy derivative ∂_E . Using the eigenvalues q_i of Q to lift the unwanted degeneracy

in the noiseless subspace is, however, non-trivial since Q has a different dimension ($2N \times 2N$) than the transmission matrix $t^\dagger t$ ($N \times N$). Accordingly, the eigenstates of Q , in general, are scattering states injected from *both* leads, whereas the eigenstates of $t^\dagger t$ are injected from the *left* lead alone. As shown below, this mismatch is conveniently resolved in the noiseless subspace where a basis of common eigenstates to both Q and $t^\dagger t$ can be found.

Due to the hermiticity of Q its eigenstates $|q_i\rangle$ form an orthogonal and complete set of states, to each of which a real “proper delay time” q_i can be assigned. In the corresponding matrix representation of this eigenproblem, $Q \vec{q}_i^{\text{in}} = q_i \vec{q}_i^{\text{in}}$, the $2N$ -dimensional time-delay eigenvectors $\vec{q}_i^{\text{in}} \equiv (\vec{q}_{i,L}^{\text{in}}, \vec{q}_{i,R}^{\text{in}})$ contain the complex coefficients of the eigenstates $|q_i\rangle$ in the flux-normalized basis of *incoming* modes in the left ($|n\rangle$) and in the right lead ($|n'\rangle$): $(\vec{q}_{i,L}^{\text{in}})_n \equiv \langle n | q_i \rangle$ and $(\vec{q}_{i,R}^{\text{in}})_{n'} \equiv \langle n' | q_i \rangle$. Correspondingly, the outgoing coefficient vectors $\vec{q}_i^{\text{out}} \equiv (\vec{q}_{i,L}^{\text{out}}, \vec{q}_{i,R}^{\text{out}})$ contain the coefficients in the basis of outgoing modes: $(\vec{q}_{i,L}^{\text{out}})_n \equiv \langle \mathcal{T}n | q_i \rangle$ and $(\vec{q}_{i,R}^{\text{out}})_{n'} \equiv \langle \mathcal{T}n' | q_i \rangle$, where \mathcal{T} is the time-reversal operator of complex conjugation ($\mathcal{T}^2 = 1$ for spinless scattering). With $\vec{q}_i^{\text{out}} = S \vec{q}_i^{\text{in}}$ and $S = S^T$ for systems with time-reversal symmetry we define an anti-unitarity operator $\Xi = \mathcal{T}S = S^\dagger \mathcal{T}$ which maps the incoming coefficients of a time-delay eigenstate onto the incoming coefficients of the corresponding time-reversed state, $(\vec{q}_i^{\text{out}})^* = \Xi \vec{q}_i^{\text{in}}$. As this operator Ξ commutes with the time-delay operator, $[\Xi, Q] = 0$ (see [14]A), any *non-degenerate* time-delay eigenstate is time-reversal invariant (up to a global phase $e^{i\alpha}$, $\alpha \in \mathbb{R}$): $\Xi \vec{q}_i^{\text{in}} = e^{i\alpha} \vec{q}_i^{\text{in}}$. For non-degenerate time-delay eigenstates whose incoming flux from one lead *exits* through both of the leads this time-reversal invariance implies that these states must also have *incoming* flux contributions from both leads. Such $2N$ -dimensional time-delay eigenvectors \vec{q}_i^{in} can thus not be reduced to an N -dimensional vector with incoming flux from the left lead alone.

This restriction is lifted in the noiseless subspace, where the *incoming* flux from one lead also *exits* through just one of the leads. Consider a noiseless time-delay eigenstate with fully transmitted incoming flux from the left lead, $t^\dagger t \vec{q}_{i,L}^{\text{in}} = \vec{q}_{i,L}^{\text{in}}$, but no incoming flux from the right lead, $\vec{q}_{i,R}^{\text{in}} = \vec{0}$. For this state, $\vec{q}_i^{\text{in}} = [\vec{q}_{i,L}^{\text{in}}, \vec{0}]$, the commutator $[\Xi, Q] = 0$ implies that the time-reversed state, $\Xi \vec{q}_i^{\text{in}} = [\vec{0}, (t \vec{q}_{i,L}^{\text{in}})^*]$, is also a time-delay eigenstate with the same eigenvalue q_i as \vec{q}_i^{in} . Being a noiseless eigenstate of $t'^\dagger t'$ with incoming flux only from the right lead, $\Xi \vec{q}_i^{\text{in}}$ is clearly orthogonal to \vec{q}_i^{in} . We thus find that such “NOiseless Time-delay Eigenstates” (NOTEs) come in pairs of two which together form the basis of a doubly degenerate subspace associated with the time-delay eigenvalue q_i . We emphasize that, in contrast to the common eigenbasis of Ξ and Q in this subspace, $[\vec{q}_{i,L}^{\text{in}}, \pm (t \vec{q}_{i,L}^{\text{in}})^*] / \sqrt{2}$, NOTEs are not time-reversal invariant. Rather, two NOTEs forming a degenerate pair

are the time-reversed of each other like a classical trajectory and its time-reversed partner. Focussing now only on NOTEs injected from the left lead, we can determine their expansion coefficients $\vec{q}_{i,L}^{\text{in}}$ with Q from Eq. (2),

$$\begin{pmatrix} Q_{11} & Q_{12} \\ Q_{21} & Q_{22} \end{pmatrix} \begin{pmatrix} \vec{q}_{i,L}^{\text{in}} \\ \vec{0} \end{pmatrix} = \begin{pmatrix} Q_{11} \vec{q}_{i,L}^{\text{in}} \\ Q_{21} \vec{q}_{i,L}^{\text{in}} \end{pmatrix} = q_i \begin{pmatrix} \vec{q}_{i,L}^{\text{in}} \\ \vec{0} \end{pmatrix}. \quad (3)$$

For the last equality to hold, the following two conditions need to be fulfilled: (i) $Q_{11} \vec{q}_{i,L}^{\text{in}} = q_i \vec{q}_{i,L}^{\text{in}}$ and (ii) $Q_{21} \vec{q}_{i,L}^{\text{in}} = \vec{0}$. This central result of our Letter implies the following operational procedure to determine the expansion coefficients of NOTEs: In a first step (i) the eigenstates of the hermitian matrix Q_{11} of dimension $N \times N$ are calculated. Out of this orthogonal and complete set of vectors the subset which, according to (ii), lies in the null-space (kernel) of Q_{21} , constitutes the desired set of common eigenstates of Q and $t^\dagger t$. In practice, condition (ii) can be conveniently verified by a null-space norm $\chi_i = \|Q_{21} \vec{q}_{i,L}^{\text{in}}\|$ which determines the degree to which the normalized vector $\vec{q}_{i,L}^{\text{in}}$ lies in the null-space of Q_{21} . The quality of a NOTE should be the better the closer this measure $\chi \in [0, \infty]$ is to zero. As the limiting value $\chi \rightarrow 0$ is only reached for exact NOTEs with wavelength $\lambda \rightarrow 0$, we need to test whether our approach works also for the realistic situation where λ has a finite value.

Consider, as a starting point for such a test, our previous argument that NOTEs can only exist in the noiseless subspace with $\tau = 0, 1$. We emphasize that this requirement, which can similarly not be fulfilled exactly for any finite value of λ , does not explicitly enter conditions (i),(ii) from above. A good indicator for the validity of our approach is thus the degree to which NOTEs with finite values of λ are, indeed, noiseless. For this purpose we calculate the eigenvectors $\vec{q}_{i,L}^{\text{in}}$ of Q_{11} [see condition (i)] and verify how the transmission of these states correlates with the corresponding null-space norm χ_i [see condition (ii)]. We find that all eigenstates of Q_{11} which closely fulfill the NOTEs condition (ii) of low χ -values are, indeed, either almost fully transmitted, $\tau \approx 1$, or fully reflected, $\tau \approx 0$. This behavior is entirely absent in Random Matrix Theory (RMT) where no phase space bands exist (a comparison of the data for the rectangular cavity with RMT is shown in Fig. 2a and in [14]B for other scattering geometries). After these consistency checks we test whether NOTEs with very low null-space norms ($\chi \lesssim 30$, see Fig. 2a) display in their wave functions the anticipated pronounced enhancements around individual bundles of classical trajectories. Our results based on the same scattering matrix data as for Fig. 1b confirm that states with such low null-space norms χ all feature highly collimated beam-like wave functions (see Fig. 2b-d and [14]E). Quite different from arbitrary noiseless states (Fig. 1a,b), NOTEs feature Husimi distributions that do not mix contributions from different phase

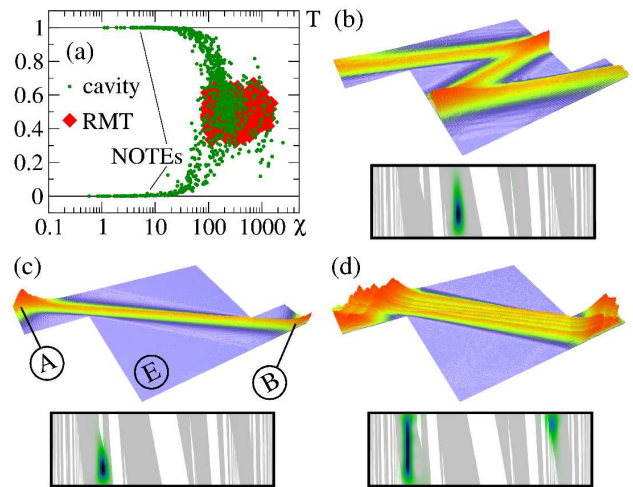


FIG. 2: (Color online) (a) Transmission T vs. null-space norm χ for eigenstates of the matrix Q_{11} in a rectangular cavity with different lead orientations (green dots). NOTEs with $\chi \rightarrow 0$ are noiseless and strongly deviate from RMT (red diamonds, see [14]B for details). (b)–(d) Wave function densities for NOTEs calculated with the same scattering matrix data as used for Fig. 1b. As demonstrated by the Husimi plots in the bottom panels, each state is located on a single classical phase space band. Null-space projections χ are (b) 4.7, (c) 6.3, (d) 6.9. The insets in (c) illustrate the possibility to use NOTEs for transferring information between a sender (A) and a receiver (B) which by-passes a potential eavesdropper (E).

space bands, thereby corroborating the successful operation of our procedure. Without exception we find that in cases where NOTEs seem to feature contributions from more than one band (as in Fig. 2d) all these bands belong to a single connected band in an extended zone scheme (like T1/T2/R2 in Fig. 1c) [12].

Our numerical results indicate furthermore that proper delay times of NOTEs do not only lift the degeneracy of noiseless states located on *different* bands, but that also the small dwell-time differences between trajectories of the *same* band do get increasingly well resolved in the limit $\lambda \rightarrow 0$. Correspondingly, we find that the proper delay times q_i of NOTEs on the *same* band are characteristically different from each other (rather than degenerate). NOTEs thus fill individual phase space bands in a well-controlled fashion. Consider, e.g., the band T1: starting from the state in Fig. 2c the proper delay times and the transverse quantization of states on this band increase (see, e.g., Fig. 2d) until, when the band is filled, the null space norm of states increases substantially (see [14]E), indicating a substantial overlap with phase space outside of the band. Such an increase in χ -values is often found to be accompanied by signatures of diffractive scattering at the sharp lead mouths (see [14]E).

Since the operational procedure presented here does not rely on any specific assumptions concerning the type of scattering in a given system, we also applied it to more

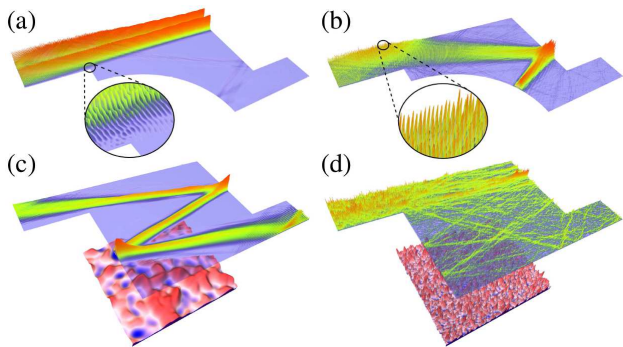


FIG. 3: (Color online) NOTEs at $k = 75.5\pi/d$ in cavities (a),(b) with a Sinai-type boundary shape and (c),(d) with a bulk disorder of amplitude $V_0/E = 0.1$ (see illustrations). The correlation of the disorder is long-range for (c) with correlation length $kr_c = 30\pi$ and short-range for (d) where $kr_c = 5\pi$. Null-space norms χ are (a) 1.7, (b) 24.8, (c) 4.9, (d) 65.7.

complex scattering geometries. Consider first the Sinai-type billiard structure in Fig. 3a,b which features chaotic classical dynamics due to scattering at the circular part of the hard wall potential. We find that NOTEs which do not have any overlap with the curved part of the boundary (see Fig. 3a) have wave functions and proper delay times as in the rectangular cavity. For comparison, we also show in Fig. 3b a state which bounces off the circular boundary. As reflected in its increased null-space norm ($\chi = 24.8$) the high instability of this state's bouncing pattern makes it much harder to resolve the (small) area of its phase space band. Consider next rectangular cavities containing a static disorder potential with correlation length r_c and an average amplitude V_0 . By studying such disordered cavities we find that our approach is restricted to the limit of weak and long-range disorder, $V_0/E \ll 1$ and $kr_c \gg 1$ (in agreement with the validity criterion for the WKB/eikonal approximation [18] and previous work [10]). Correspondingly, for the same fixed disorder amplitude ($V_0/E = 0.1$) the z -shaped scattering state from Fig. 2b survives in the presence of long-range disorder (see Fig. 3c), whereas no such state exists for short-range correlations (see Fig. 3d for the state with the closest time-delay value and [14]B,E for more details).

We have performed additional tests (see [14]C) to verify that all NOTEs which we find within the above limits are associated with individual classical trajectory bundles. This feature allows for a WKB/eikonal-type ansatz for the transmission matrix of NOTEs, $t \approx \vec{q}_{i,R}^{\text{out}} e^{i\mathcal{S}_b(E)/\hbar} \vec{q}_{i,L}^{\text{in}\dagger}$, in which the only part with a significant energy-dependence is the action phase, $\mathcal{S}_b(E) = \int_b \vec{k} d\vec{l}$, accumulated along bundle b . We show in [14]D that this ansatz fulfills the defining conditions for NOTEs (i),(ii) from above.

We believe that our results open up many interesting possibilities for the experiment, where the cavities considered here could, e.g., be an acoustic resonator (like a

room) or an electromagnetic scatterer (like closely spaced buildings). In both these cases the collimated wave functions associated with NOTEs might allow to transfer information between a sender (A) and a receiver (B) such that the power to generate the signal is minimized and the transmitted signal is kept out of reach of an eavesdropper (E) (see illustration in Fig. 2c). In this sense NOTEs offer clear advantages over arbitrary noiseless scattering states that do not display such beam-like wave functions in general (see, e.g., Fig. 1b). NOTEs may also have interesting connections to phenomena in closed/decaying systems [15–17].

In summary, we present an operational procedure for constructing scattering states which follow classical bouncing patterns in coherent transport through cavities or complex scattering landscapes. In analogy to WKB/eikonal theory we find that such ray-optical/beam-like scattering states are determined by the condition of a fixed scattering time-delay. Our procedure is generally applicable to different types of wave scattering (acoustic, electro-magnetic, quantum etc.) and relies solely on the knowledge of the scattering matrix.

We wish to thank F. Aigner, J. Burgdörfer, A. Cresti, and A. Foerster for helpful discussions. Support by the WWTF and computational resources by the Vienna Scientific Cluster (VSC) are gratefully acknowledged.

* Corresponding author: stefan.rotter@tuwien.ac.at

- [1] S. M. Popoff, *et al.*, Phys. Rev. Lett. **104**, 100601 (2010).
- [2] I. M. Vellekoop and A. P. Mosk, Phys. Rev. Lett. **101**, 120601 (2008).
- [3] Z. Yaqoob *et al.*, Nature Photonics **2**, 110 (2008).
- [4] I. M. Vellekoop, A. Lagendijk, and A. P. Mosk, Nature Photonics **4**, 320 (2010).
- [5] P. Ehrenfest, Z. Physik **45**, 455 (1927).
- [6] P. G. Silvestrov, M. C. Goorden, and C. W. J. Beenakker, Phys. Rev. B **67**, 241301 (2003).
- [7] J. Tworzydło *et al.*, Phys. Rev. B **68**, 115313 (2003).
- [8] P. Jacquod and E. V. Sukhorukov, Phys. Rev. Lett. **92**, 116801 (2004).
- [9] P. Jacquod and R. S. Whitney, Phys. Rev. B **73**, 195115 (2006).
- [10] S. Rotter, F. Aigner, and J. Burgdörfer, Phys. Rev. B **75**, 125312 (2007).
- [11] S. Rotter, *et al.*, Phys. Rev. B **62**, 1950 (2000); **68**, 165302 (2003).
- [12] L. Wirtz, J.-Z. Tang, and J. Burgdörfer, Phys. Rev. B **56**, 7589 (1997).
- [13] L. Reichl, *The transition to chaos* (Springer, 2004) 2nded.
- [14] See supplemental material provided below.
- [15] E. G. Vergini *et al.* EPL **89** 40013 (2010).
- [16] M. Kopp and H. Schomerus, Phys. Rev. E **81**, 026208 (2010).
- [17] H. E. Türeci *et al.*, Opt. Expr. **10**, 752 (2002).
- [18] R. J. Glauber, *Lectures in Theoretical Physics* (New York: Interscience, 1959), vol. 1, p. 315.

Supplemental material for "Generating particle-like scattering states in wave transport"

Stefan Rotter, Philipp Ambichl, and Florian Libisch
Institute for Theoretical Physics, Vienna University of Technology, A-1040 Vienna, Austria, EU
(Dated: November 10, 2018)

A. TIME-REVERSAL OPERATOR

In the main article we introduce the anti-unitary time-reversal operator $\Xi = \mathcal{T}S$ which maps the incoming coefficients of a scattering state onto the incoming coefficients of the corresponding time-reversed state. For time-reversal invariant systems like the ones we study the scattering matrix S is unitary symmetric such that the time-reversal operator Ξ can also be written as follows: $\Xi = S^\dagger \mathcal{T}$. This identity can be conveniently used to show that Ξ commutes with the Wigner-Smith time-delay operator Q which, due to its Hermiticity, satisfies the following identities: $Q = i\hbar(\partial_E S^\dagger)S = -i\hbar S^\dagger(\partial_E S)$. In particular, we have:

$$\begin{aligned} [Q, \Xi] &= \{i\hbar(\partial_E S^\dagger)S\} S^\dagger \mathcal{T} - S^\dagger \mathcal{T} \{-i\hbar S^\dagger(\partial_E S)\} = \\ &= i\hbar \{(\partial_E S^\dagger)SS^\dagger \mathcal{T} - S^\dagger S \mathcal{T}(\partial_E S)\} = \\ &= i\hbar \{(\partial_E S^\dagger)\mathcal{T} - (\partial_E S^\dagger)\mathcal{T}\} = 0. \end{aligned} \quad (\text{E.1})$$

B. STATISTICAL ANALYSIS OF NOTES

Since we expect the presence of NOTES in a given scattering system to depend on non-universal, system specific scattering processes, we should find no NOTES in a system described by an entirely random scattering matrix as in Random Matrix Theory (RMT). Whereas RMT is thus not a suitable framework for studying NOTES, the differences that appear between an RMT description and a full numerical solution of a non-universal scattering system will be very instructive for characterizing NOTES in detail.

Random Matrix Model

For a suitable RMT model of scattering which provides also the Wigner-Smith time delay matrix we follow the so-called "Heidelberg approach" reviewed, e.g., in [1]. This approach links the scattering matrix S of a system with the Hamiltonian H of the corresponding closed cavity through the coupling matrix W between the discrete bound states in the cavity and the continuum in the attached leads,

$$S(E) = I - 2\pi i W^\dagger \frac{1}{E - H + i\pi W W^\dagger} W. \quad (\text{E.2})$$

For time-reversal invariant systems the Hamiltonian matrix H is taken from the Gaussian orthogonal ensemble ($\beta = 1$). The mean spacing of the energy eigenvalues of H is adjusted to match the corresponding mean level spacing $\Delta E = 2\pi/A$ of our cavities with size A . (Note that the chaotic cavities we study have a smaller scattering area A and are thus compared with a different RMT ensemble than the regular and the disordered cavities.) The mean absolute value of the random coupling matrix elements of W is adjusted such as to produce a scattering matrix S with, on average, balanced total transmission and reflection, $\langle T \rangle \approx \langle R \rangle \approx \langle T' \rangle \approx \langle R' \rangle \approx N/2$ [2].

For calculating the Wigner-Smith time-delay matrix based on Eq. (E.2), $Q = i\hbar(\partial_E S^\dagger)S$, we make the usual assumption [1] that the coupling matrix elements in W are only weakly energy-dependent such that the derivative $\partial_E S^\dagger$ affects only the explicit energy dependence in the denominator of Eq. (E.2). To check our results we have verified that the Wigner-Smith time-delay matrix Q obtained in this way gives rise to eigenvalues q_i which are statistically distributed according to the RMT predictions put forward in [3] (not shown).

Comparison of numerical data with RMT

It is now of interest to compare the results obtained with this RMT approach with those from our numerical calculations for the regular, chaotic, and disordered cavities. The RMT data was produced based on an ensemble with altogether 20 random scattering matrices following Eq. (E.2). To obtain a comparatively large ensemble of statistical data also for the cavities, we performed the numerical wave calculations with 20 different disorder realizations (for the disordered cavities) and with 20 different lead configurations (for the regular and the chaotic cavity). In the latter case, we shifted the right lead in equidistant steps from the bottom to the top position (the left lead was kept fixed at the top position). To counterbalance the increased numerical effort necessary for calculating such ensembles of cavities, we reduced the wavenumber from $k = 75.5\pi/d$ (as used for the plots in the main text) to $k = 45.5\pi/d$.

In both the RMT and the cavity calculations we focused, in particular, on the eigenstates $\vec{q}_{i,L}^{\text{in}}$ of Q_{11} which, according to condition (i) in our procedure (see main text), are the key ingredients for NOTES. In Fig. E.1 we plot the total transmission of these states as a function of

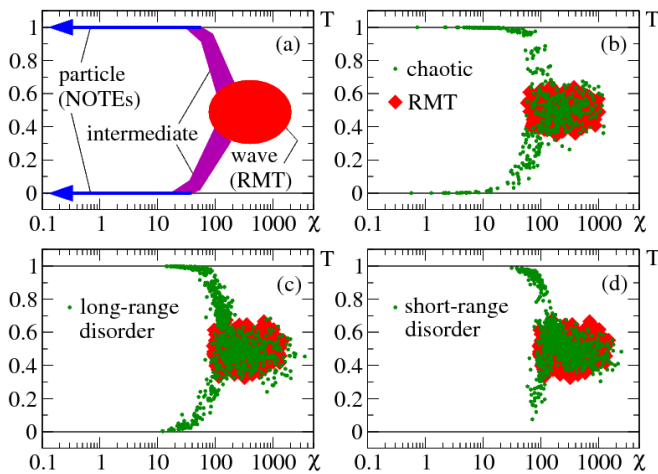


Fig. E.1: Transmission versus null-space norm χ for eigenstates of the submatrix Q_{11} of the Wigner-Smith time-delay matrix Q (wave number $k = 45.5\pi/d$). (a) Schematic of the results shown in Fig. 2a (main text) to illustrate the crossover between particle/classical and wave/quantum scattering. (b)-(d) Same as Fig. 2a (main text) for (b) the Sinai-type cavity with chaotic classical dynamics as well as for weakly disordered cavities ($V_0 = 0.1E$) with (c) long-range ($kr_c = 15\pi$) and (d) short-range ($kr_c = 2.5\pi$) disorder. The red diamonds show the data obtained from the RMT calculations from altogether 20 randomly assembled S -matrices (for better visibility we use an increased symbol size for the RMT data). Strong deviations between the cavity and the RMT data are observed which point to the presence of NOTEs with small null-space norms $\chi \rightarrow 0$ and noiseless transmission $T(1-T) \rightarrow 0$. The presence of a disorder potential (in particular, with short-range correlation) shifts the cavity data towards the RMT distribution and strongly reduces the amount and the quality of NOTEs.

the corresponding null-space norm $\chi = \|Q_{21}\vec{q}_{i,L}^{\text{in}}\|$ which, according to condition (ii) measures whether a state can be identified as a NOTE. In this plot already a number of important features become apparent: the data from the RMT calculations (red diamonds) accumulate in a very restricted region of the parameter space: the norm χ of the RMT states stays within a restricted interval of χ and their transmission clusters very strongly around the mean transmission $T = 0.5$. This situation is quite different for the cavities: whereas the upper bound of the norm χ is comparable to the corresponding RMT value, the lower bound of χ is more than two orders of magnitude smaller than in RMT, suggesting a strongly non-universal behavior. Furthermore we observe that states with very low values of the norm χ are all clustered around the noiseless transmission values very close to $T = 0$ and $T = 1$.

This observation demonstrates that, indeed, eigenstates of Q_{11} with a vanishing nullspace norm [$\chi \rightarrow 0$] have noiseless transmission [$T(1-T) \rightarrow 0$]. Equivalently, each scattering state injected from just the left lead [i.e., with $\vec{q}_{i,R}^{\text{in}} = 0$] which is a time-delay eigenstate is found to

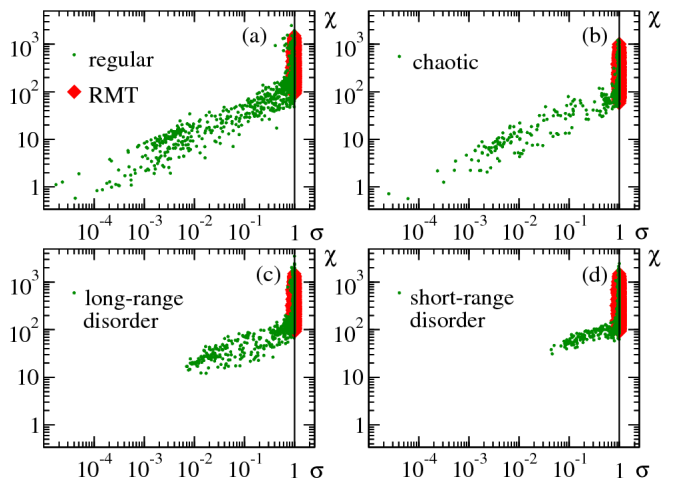


Fig. E.2: Null-space norm $\chi = \|Q_{21}\vec{q}_{i,L}^{\text{in}}\|$ versus noiseless norm $\sigma = 4T(1-T)$ for the four different cavity types investigated. The same data set and color coding is used as in Fig. E.1. A strong positive correlation between the two norms χ and σ is visible for all data points that are strongly non-universal, i.e., for parameter values that are different from those where the RMT results cluster (see red diamonds).

be either fully transmitted or fully reflected. NOTEs are thus, indeed, noiseless. We can further write the transmission T of a NOTE as $T = \sum_i |c_i|^2 \tau_i$, where the τ_i are the transmission eigenvalues of $t^\dagger t$ and the c_i are the expansion coefficients of the NOTE in the eigenbasis of $t^\dagger t$. From this we conclude that the noiseless transmission values of NOTEs, $T \approx 0$ ($T \approx 1$), imply that NOTEs can only have non-negligible expansion coefficients c_i for those transmission eigenvalues τ_i which are themselves noiseless, $\tau_i \approx 0$ ($\tau_i \approx 1$). NOTEs can thus only be composed of noiseless transmission eigenchannels.

We emphasize that the strong correlation between time-delay eigenstates and noiseless scattering (which does not explicitly enter our construction of NOTEs) persists here in the limit of finite channel numbers where neither the null-space norm χ is exactly 0 nor the transmission T is exactly noiseless for any state. To highlight this strong correlation we show in Fig. E.2 the null-space norm χ of Q_{11} eigenstates as a function of $\sigma = 4T(1-T)$, which measure for noiseless scattering can vary between 0 and 1. For all states which display non-universal behavior (deviating from the RMT-result) a strong positive correlation between the two measures χ and σ is observed, suggesting that we can use these two measures interchangeably for testing the quality of a NOTE. We have checked explicitly that the statistical spread in the correlation between χ and σ (see Fig. E.2) is further reduced when considering states on the same phase space band.

The statistical data shown in Fig. E.1 and Fig. E.2 also demonstrate that NOTEs are completely absent in the RMT description along Eq. (E.2). This observation

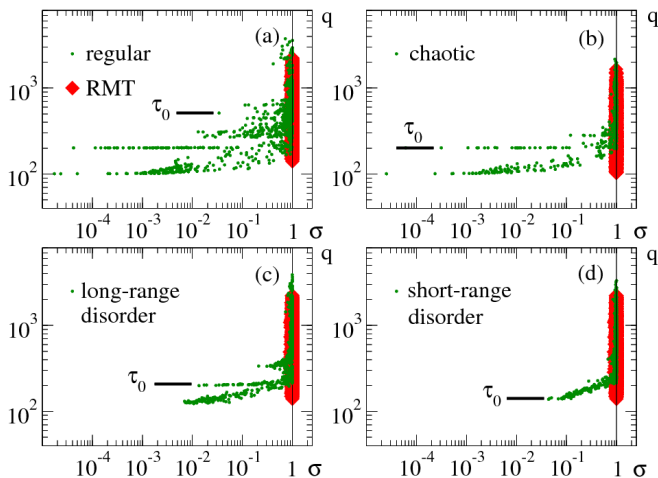


Fig. E.3: Eigenvalues q_i of Q_{11} versus noiseless norm σ of the corresponding eigenvectors $\tilde{q}_{i,L}^{\text{in}}$. The same data set and color coding is used as in Fig. E.1. As expected from our model, all states with a small noiseless norm σ correspond to short delay-time values q_i . A clustering of these q_i -values around the classical values belonging to individual phase space bands is clearly observed. Note, e.g., that a delay time of 100 (200) corresponds to a single (double) traversal of the cavity along the upper cavity boundary in those cavity configurations where the right lead is (is not) located at the top-most position. The maximum delay-time τ_0 where such non-universal deviations with $\sigma < 0.1$ occur are indicated by the black horizontal bars. The values of τ_0 are reduced in chaotic vs. regular ballistic cavities and in short-range vs. long-range disordered cavities.

is perfectly in line with the expectation that the presence of NOTES requires extended bands in phase space. As such non-universal features are clearly absent in the RMT description, this model does not give rise to any NOTES. Rather, the eigenstates of the random matrix Q_{11} do not constitute a preferred basis in terms of transmission (as opposed to the eigenstates of $t^\dagger t$). Their transmission values thus cluster around the average value $T \approx 0.5$ and are strongly suppressed near the noiseless values $T \approx 0, 1$. As discussed in the main part of the paper, one can show by employing the time-reversal operator Ξ that such states which lie outside the noiseless subspace can never be time-delay eigenstates when injected from just one of the leads. Correspondingly, the Q_{21} null space norm χ of these RMT states always remains larger than the (small) χ -values of NOTES.

From the above results we conclude that the noiseless eigenstates of Q_{11} are NOTES for which the corresponding eigenvalues q_i of Q_{11} are time-delay values. Following our model we expect that these time-delay eigenvalues correspond to the time spent in the cavity when scattering *along a given trajectory bundle* (see section C for more details). Consequently, all states that belong to the same bundle should feature similar values of q_i , which we expect to lead to a clustering of q_i -values around the classical time delay values of those trajectory bundles which

can be fully resolved by a scattering state. As, in turn, the degree of this resolution is measured by the noiseless norm σ (or, alternatively, by the null-space norm χ) it is instructive to plot the eigenvalues q_i of Q_{11} as a function of these norms σ (or χ). The resulting plot shown for the noiseless norm σ in Fig. E.3 nicely confirms the expected behavior: we first observe that no states with both very long time-delays *and* small σ -values are found, in correspondence with the expectation that NOTES can only form on short-lived/stable phase space bands. States with small norm values σ show the most pronounced deviations from RMT and correspond exclusively to short-lived states with time-delay values on the lower end of the entire distribution. For a single cavity these non-universal q_i -values cluster along horizontally elongated regions, corresponding to states on the same phase space band. For such states the time-delay values q_i are similar, but the norms σ vary considerably, depending on the overlap of a state with regions outside the band. In Fig. E.3 such a clustering of values is still visible but blurred due to the different lead configurations that enter the statistical data set. Those NOTES out of this set with the lowest values of χ correspond to scattering states which propagate solely along the upper cavity boundary where the focussing is enhanced by the top cavity wall. In contrast, all of these non-universal features are drastically reduced for states with a norm σ near the maximum value 1.

Signatures of regular/chaotic/disorder scattering

Since NOTES are highly non-universal and system-specific scattering states, their number and their quality should depend significantly on the type of scattering present in a given scattering region. To investigate this issue in more detail we calculated all of the above plots for the regular, chaotic and disordered cavities, respectively. As a measure for the influence of these different scattering mechanisms we introduce a critical time scale τ_0 which represents the maximal time up to which time-delay eigenvalues of a given quality ($\sigma_0 = 0.1$) exist for a given system. As this time scale τ_0 measures for how long scattering states follow the classical bouncing patterns of NOTES (see section C) τ_0 can loosely be associated with the Ehrenfest time (see Refs. [5-10] in the main paper).

In all of the above plots we consistently find that the strongest deviations from RMT occur for the regular cavity which, correspondingly, also features the largest value of τ_0 (see black horizontal bars in Fig. E.3). Note that for the regular cavity deviations from RMT do persist to a certain degree also for states with time-delays longer than τ_0 , indicating that in regular cavities also very long-lived states may carry non-universal features. Comparing these results with those for the chaotic cavity we observe the following interesting behavior: whereas states

with the shortest time-delays feature very similar values of the norm σ in the regular and the chaotic cavities, τ_0 is considerably shorter for the chaotic scatterer than for the regular one. This can be intuitively explained by the fact that short-lived NOTES which do not have any overlap with the circular part of the boundary in the chaotic dot are the same as the corresponding states in the regular cavity. Those very stable states corresponding to the smallest σ values thus appear in both cavity types with similar parameter values. Longer-lived states do eventually also explore the circular boundary part in the chaotic cavity which leads to increased wave spreading and thus to a reduced value of τ_0 . In the cavity with long-range disorder the situation is again conspicuously different from the chaotic cavity, although both types of cavities give rise to classical chaotic scattering: in the long-range disordered cavity even the most short-lived states are drastically affected by the disorder since it is contained in the bulk and affects all scattering states (in contrast to the chaotic cavity where the circular boundary part can be avoided). Correspondingly, the minimum value of the norm σ is much higher for the disordered cavity than for both the regular and the chaotic cavity. When changing the correlation length of the disorder to smaller length scales (with the disorder amplitude remaining unchanged at $V_0/E = 0.1$) the effect of the disorder is further increased: here even the states with the shortest delay time have σ values which are three orders of magnitude larger than in the ballistic cavities without disorder. Also τ_0 is here much smaller than in all other cavity types. This behavior can be attributed to the effect of stochastic scattering which is induced whenever the correlation length of the disorder is of comparable magnitude or smaller than the wavelength.

NOTEs and general time-delay eigenstates

In the main part of the article we argue that NOTES should appear as a special subset of eigenstates of the Wigner-Smith time-delay operator Q . A convenient way to test this relation between NOTES and general time-delay eigenstates is to compare the eigenvalues and eigenvectors of the submatrix Q_{11} (which we use to generate NOTES) with those of the general Wigner-Smith time-delay matrix Q . In particular, we expect that the eigenvectors and eigenvalues belonging to a NOTE (i.e., for which $\chi, \sigma \rightarrow 0$) should emerge for both matrices, whereas the remaining eigenstates (with higher values of χ, σ) may again be close to the corresponding RMT values for each of these two matrices. To check whether this expected behavior is, indeed, fulfilled consider Fig. E.4: this plot shows the eigenvalues q_i as a function of the noiseless norm σ obtained here from the entire matrix Q rather than only from Q_{11} as in Fig. E.3. The two sets of eigenstates from Q and Q_{11} are of different size since

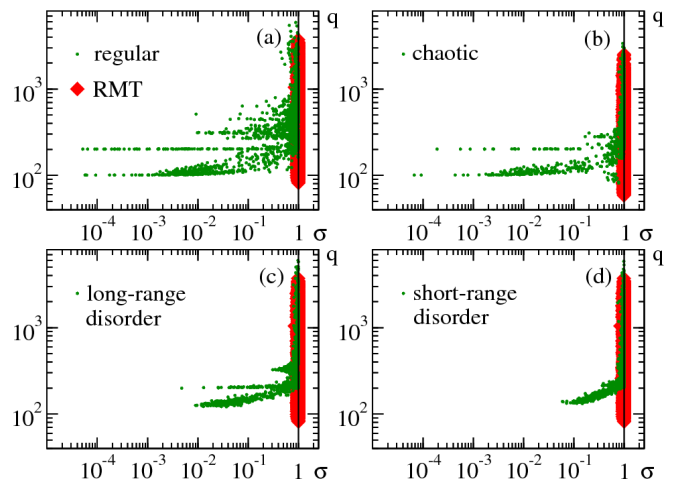


Fig. E.4: Same as Fig. E.3 but with the time-delay eigenvalues q_i and the noiseless norm σ determined from the eigenproblem for the whole Wigner-Smith matrix Q (see text for details). As predicted by our model, a clear correspondence with Fig. E.3 can be observed for small values of σ . This indicates that NOTES as identified by the procedure proposed in the main text naturally emerge as eigenstates of the Wigner-Smith time-delay matrix.

the eigenvectors \vec{q}_i^{in} of Q contain the incoming mode coefficients from both leads, $\vec{q}_i^{\text{in}} = (\vec{q}_{i,L}^{\text{in}}, \vec{q}_{i,R}^{\text{in}})$, not just from the left lead alone. We thus calculate the norm $\sigma = 4T(1 - T)$ for Fig. E.4 just based on the transmission T associated with the (normalized) injection coefficients from the left lead, i.e., with $\vec{q}_{i,L}^{\text{in}} / \|\vec{q}_{i,L}^{\text{in}}\|$. Since we expect NOTES to appear in the eigenvectors of Q as a near degenerate doublet (see main text) the normalization removes here the effect of mixing between these two degenerate states. Figure E.4 obtained in this way displays the same characteristic and non-universal features as Fig. E.3. The way in which these features are similar in both plots corroborates our approach.

The small differences between Figs. E.3, E.4 which remain for small values of σ can be well described with the help of degenerate perturbation theory (not shown). In this description the “perturbation” is given in terms of the off-diagonal matrices Q_{12}, Q_{21} which mix the eigenstates of the “unperturbed” matrices Q_{11}, Q_{22} . Eigenstates and eigenvalues of Q_{11} thus get perturbed through admixtures from other states which, in further consequence, lead to the above differences. In turn, these admixtures should vanish when the perturbation of a Q_{11} -eigenstate $\vec{q}_{i,L}^{\text{in}}$ by the matrices Q_{12} or, equivalently, by Q_{21} goes to zero. Note that this situation is exactly realized when the null-space norm $\chi = \|Q_{21}\vec{q}_{i,L}^{\text{in}}\|$ (or, equivalently, the noiseless norm σ , see discussion above) goes to zero. This reasoning not only substantiates the fact that the norms χ and σ are a suitable means to measure the quality of a NOTE but also that in the numerically unreachable limit of infinitely many lead modes ($N \rightarrow \infty$)

we should expect the Wigner-Smith time-delay matrix to feature exactly degenerate pairs of NOTES.

C. NOTES AND CLASSICAL TRAJECTORY BUNDLES

An interesting question to ask is whether all NOTES we find are associated with classical trajectory bundles and vice versa. To answer this question we have performed a number of tests: our work builds on the established result from the literature (see, e.g., [4]) according to which phase space bands with a size larger than Planck's constant give rise to noiseless scattering channels. In the weakly disordered regime (which we consider) each of these bands can be associated with a bundle of classical trajectories of equivalent topology and similar length (a situation which is in general not fulfilled for strongly disordered systems). To verify whether all NOTES are associated with such classical trajectory bundles we thus need to test if the NOTES generated with our procedure [see conditions (i),(ii) on page 3 in the main paper text] are composed exclusively of noiseless scattering channels. As demonstrated in section B (see, in particular Figs. E.1, E.2) all NOTES which we find in the ballistic structures (regular and chaotic), indeed, have this property. We also find that in the weakly disordered structures where such trajectory bundles are disturbed, NOTES are of considerably lower quality. Furthermore, the quality and quantity of NOTES correlates strongly with the area of a given phase space band: consider, e.g., that no NOTES are found with very large time-delays (see Figs. E.3, E.4) as these are associated with very small phase space bands. We conclude from these observations that all NOTES we find can, indeed, be associated with classical trajectory bundles.

The above arguments still leave open whether each NOTE can be associated with only a single or multiple trajectory bundles. Since NOTES are time-delay eigenstates and different bundles have, in general, different time-delays our procedure should yield only a single bundle per NOTE already by construction. To test whether this expectation is, indeed, fulfilled we performed the following additional tests: We have checked that each time-delay eigenvalue q_i associated with a NOTE in the regular cavity corresponds to a classical time-delay value from a single classical phase space band: Based on the classical dynamics in a rectangular cavity the product of a proper delay time q_i with the eigenstate's average longitudinal velocity, $\langle |v_x^i| \rangle = \hbar \langle |k_x^i| \rangle / m$, must be an integer multiple of the cavity width W , corresponding to the number M of the state's left-right cavity traversals, $q_i |v_x^i| = MW$. With the average longitudinal momentum $\langle |k_x^i| \rangle$ of state i being determined as follows, $\langle |k_x^i| \rangle = \sum_{n=1}^N |(\vec{q}_{i,L}^{\text{in}})_n|^2 \sqrt{k^2 - (n\pi/d)^2}$, we find this criterion to be fulfilled with a relative error below 2% by all

the NOTES for which $\chi \lesssim 20$. This result confirms that for the rectangular cavity our numerical procedure yields proper delay times in very good agreement with classical expectation. In the chaotic cavity we have checked that NOTES which have no overlap with the circular boundary feature a one-to-one correspondence with the equivalent states in the regular cavity (both in terms of the time-delay eigenvalue and in terms of the wave function). For the remaining NOTES in the chaotic cavity (which do have an overlap with the circular boundary) and for all NOTES in the disordered cavities we have checked explicitly with the help of the corresponding scattering wave functions that these NOTES all feature highly colimated wave function patterns as expected for states that are supported by classical trajectory bundles. Details can be found in section E, where we have provided the wave function patterns of NOTES on specific phase space bands (in the ballistic cavities) and all NOTES with $\chi \lesssim 30$ in the disordered cavities.

Whereas the above tests suggest that each NOTE we found is associated with a single phase space band/trajectory bundle this association does not always hold in the opposite direction: as stated above, NOTES can only be formed on phase space bands with a size larger than h (a condition which we have explicitly verified in an earlier paper [5]). A further restriction to form NOTES on such noiseless channels comes from the well-defined time-delay associated with NOTES. This requirement imposes an additional constraint which makes it harder for NOTES to fit on a given phase space band as compared to the transmission eigenstates of $t^\dagger t$. Correspondingly, we find that the transmission of NOTES is generally not as noiseless as that of the transmission eigenstates (not shown).

We mention, parenthetically, that imperfections both in the formation of noiseless channels and NOTES are mostly reflected by those states labeled as "intermediate" in Fig. E.1a: these states deviate from RMT statistics but do not have a good quality as NOTES. Such intermediate states are found to persist in the presence of weak disorder (Fig. E.1c,d).

D. WKB/EIKONAL ANSATZ FOR NOTES

In the main part of the paper we showed that NOTES are defined by the two conditions (i) $Q_{11} \vec{q}_{i,L}^{\text{in}} = q_i \vec{q}_{i,L}^{\text{in}}$ and (ii) $Q_{21} \vec{q}_{i,L}^{\text{in}} = \vec{0}$. In this part of the appendix we investigate how these equations can be satisfied, based on the observation from section C that NOTES are time-delay eigenstates located on individual phase space bands. We assume, for simplicity, that we are dealing with a transmission band, leading to a fully transmitted NOTE. Our arguments can, however, be applied to reflection bands as well.

Consider first the eigenproblem in (i): $Q_{11} \vec{q}_{i,L}^{\text{in}} =$

$i\hbar(r^\dagger r + t^\dagger t) \vec{q}_{i,L}^{\text{in}} = q_i \vec{q}_{i,L}^{\text{in}}$. Using the property that $\vec{q}_{i,L}^{\text{in}}$ is a fully transmitted noiseless state, $t^\dagger t \vec{q}_{i,L}^{\text{in}} = \vec{q}_{i,L}^{\text{in}}$, we have $r^\dagger r \vec{q}_{i,L}^{\text{in}} = r^\dagger \vec{0} = \vec{0}$, leaving us with $Q_{11} \vec{q}_{i,L}^{\text{in}} = i\hbar t^\dagger t \vec{q}_{i,L}^{\text{in}} = q_i \vec{q}_{i,L}^{\text{in}}$ for the evaluation of which we perform a singular value decomposition (SVD) of $t = \sum_i t_i$ with $t_i = \vec{u}_i \sigma_i \vec{v}_i^\dagger$. Here the right-singular vectors $\vec{v}_i = \vec{\tau}_i^{\text{in}}$ are the eigenvectors of $t^\dagger t$, the left-singular vectors $\vec{u}_i = (\vec{\tau}_i^{\text{in}})^*$ are the eigenvectors of $tt^\dagger = (t^\dagger t)^*$, and the singular values are the square roots of the corresponding transmission eigenvalues, $\sigma_i = \sqrt{\tau_i} \in [0, 1]$. In wave transport through complex scattering landscapes the non-deterministic singular values $0 < \sigma_i < 1$ and their corresponding singular vectors \vec{v}_i and \vec{u}_i feature a very strong energy dependence as reflected, e.g., in the familiar conductance fluctuations. In the degenerate noiseless subspace where $\sigma_i = 0, 1$ the situation is more complicated: states which are noiseless due to an appropriate interference of path contributions (like in Fig. 1a) also feature a significant energy dependence induced by multi-path interference. For those states that are noiseless due to a resolution of the underlying classical phase space (like in Fig. 1b) the singular values σ_i all stay at the energy-independent degenerate values of $\sigma_i = 0, 1$ (see, e.g., [4]). Since the corresponding singular vectors are, typically, distributed over several transmission (reflection) bands for $\sigma_i = 1$ ($\sigma_i = 0$) their energy-dependence is not well defined unless we fix this distribution. As we argue above, a distribution where each state is located on a single band can be achieved by demanding that the noiseless vectors \vec{v}_i are NOTEs, $\vec{v}_i = \vec{q}_{i,L}^{\text{in}}$ and $\vec{u}_i = t \vec{q}_{i,L}^{\text{in}}$. On a single band all involved trajectories will accumulate a very similar phase, leading to energy-independent constructive interference such that the incoming/right singular vectors have only a very weak energy dependence, $\partial_E \vec{v}_i \approx \vec{0}$. In this relation the arbitrary global phase that we are free to choose in any SVD was fixed for the vector \vec{v}_i such as to minimize its energy-dependence. This condition, in turn, also determines the corresponding outgoing/left singular vector, $\vec{u}_i = \vec{u}_i^0 e^{i\phi_b(E)}$, to consist of an energy-independent part, $\partial_E \vec{u}_i^0 \approx \vec{0}$, and an energy-dependent phase shift, $e^{i\phi_b(E)}$. The phase shift $\phi_b(E) = \mathcal{S}_b(E)/\hbar - \pi\mu_b/2$ can be associated with the action $\mathcal{S}_b(E) = \int_b \vec{k} d\vec{l}$ and the Maslov index μ_b accumulated along the phase space band b . With the transmission amplitudes for the transmitted NOTEs now being $t_i = \vec{q}_{i,R}^{\text{in}*} e^{i\phi_b} \vec{q}_{i,L}^{\text{in}\dagger}$, we can further simplify condition (i): $Q_{11} \vec{q}_{i,L}^{\text{in}} = i\hbar t^\dagger t \vec{q}_{i,L}^{\text{in}} = i\hbar [\partial_E(t^\dagger t \vec{q}_{i,L}^{\text{in}}) - t^\dagger \partial_E(t \vec{q}_{i,L}^{\text{in}})] =$

$(\partial_E \mathcal{S}_b) \vec{q}_{i,L}^{\text{in}}$, from which we obtain the time-delay eigenvalue $q_i = \partial_E \mathcal{S}_b$, in full analogy to the one-dimensional case [6]. Similarly, condition (ii) reads: $Q_{21} \vec{q}_{i,L}^{\text{in}} = i\hbar r'^\dagger t \vec{q}_{i,L}^{\text{in}} = i\hbar [\partial_E(r'^\dagger t \vec{q}_{i,L}^{\text{in}}) - r'^\dagger \partial_E(t \vec{q}_{i,L}^{\text{in}})] = i\hbar [\partial_E(r'^\dagger t \vec{q}_{i,L}^{\text{in}}) - (\partial_E \mathcal{S}_b) r'^\dagger t \vec{q}_{i,L}^{\text{in}}]$, which expression must be zero since the unitarity of the S -matrix implies $r'^\dagger t = -t'^\dagger r$ and $t'^\dagger r \vec{q}_{i,L}^{\text{in}} = 0$ for a noiseless transmission state.

We have thus verified that WKB/eikonal-type scattering states which are characterized by their phase shift accumulated along a given trajectory bundle satisfy the two defining equations (i),(ii) which we have put forward to construct NOTEs.

E. WAVE FUNCTION IMAGES

In the figures attached below we provide a number of wave function images as obtained for the four different cavity types discussed in the main article. In the regular and chaotic cavity we show all states belonging to a specific phase space band: Figs. E.5, E.6 illustrate how NOTEs systematically increase their transverse quantization until, when a band is filled, overlap with phase space regions outside this band lead to a significant drop in the quality of NOTEs. For the disordered cavities we display all wave function patterns with a quality below $\chi \lesssim 30$: Figs. E.7, E.8 show that all states of this quality still feature very collimated wave functions in spite of the presence of weak disorder. Note that in the cavity with long-range correlations in the disorder the number of NOTEs of this quality is much higher than with short-range disorder.

-
- [1] Y. Fyodorov and H.-J. Sommers, J. Math. Phys. **38**, 1918 (1997).
 - [2] K. Pichugin, H. Schanz, P. Šeba, Phys. Rev. E **64**, 056227 (2001).
 - [3] H. J. Sommers, D. V. Savin, and V. V. Sokolov, Phys. Rev. Lett. **87**, 094101 (2001).
 - [4] H. Schomerus and P. Jacquod, J. Phys. A **38**, 10663 (2005).
 - [5] S. Rotter, F. Aigner, and J. Burgdörfer, Phys. Rev. B **75**, 125312 (2007).
 - [6] L. Reichl, *The transition to chaos* (Springer, New York, 2004) 2nd ed.

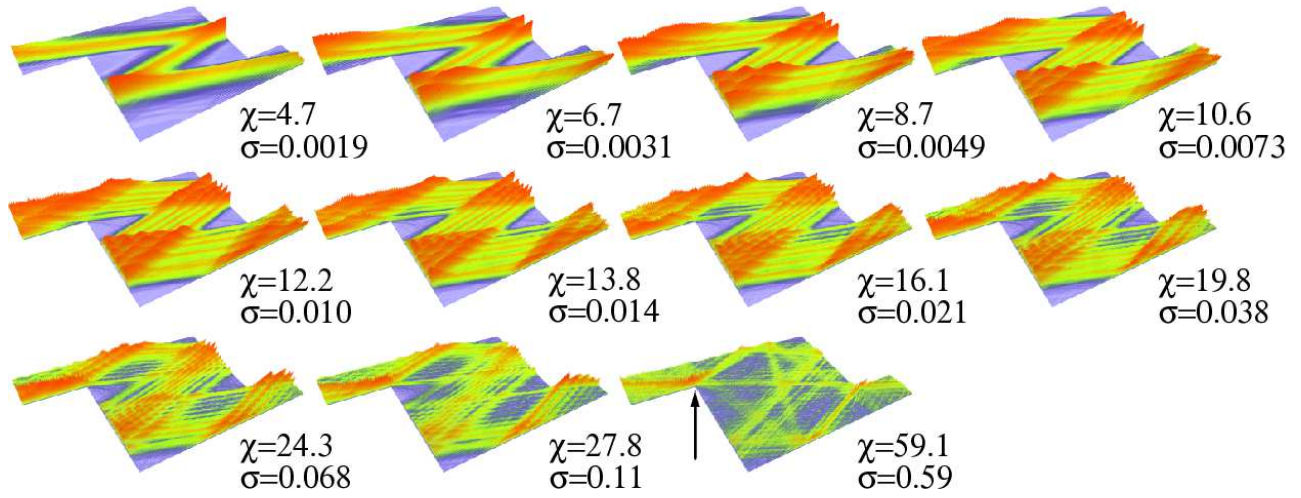


Fig. E.5: Wave function densities of NOTEs in the rectangular cavity at wave number $k = 75.5\pi/d$: States associated with the transmission band T2 (see Fig. 1c in the main text) are shown with their respective null-space and noiseless norms χ, σ . With increasing transverse quantization the quality of states (as measured by χ, σ) deteriorates monotonically. This decrease in the quality of NOTEs is accompanied by the appearance of diffraction effects at the sharp lead mouth (see arrow in the bottom row).

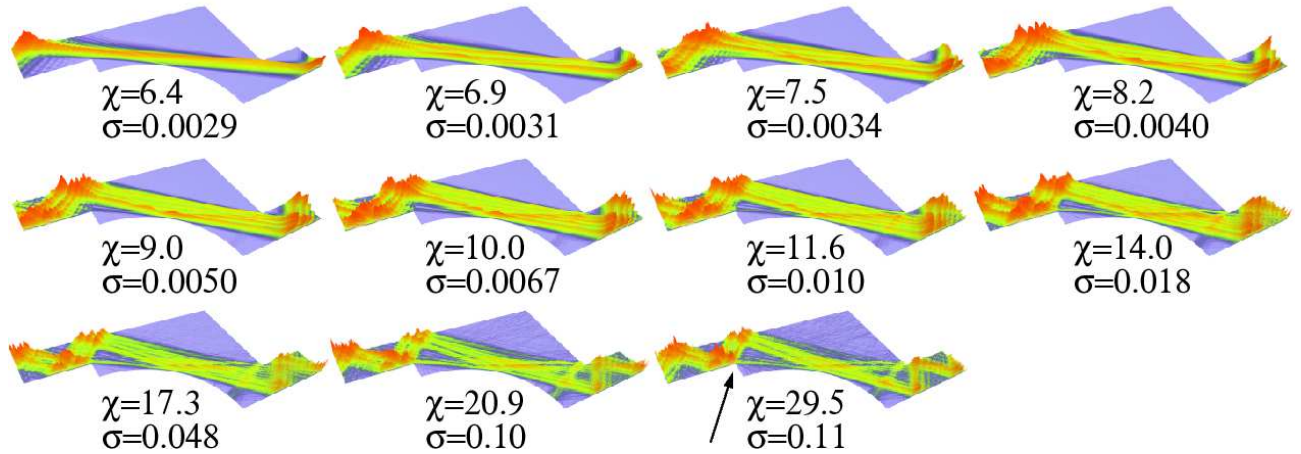


Fig. E.6: Wave function densities of NOTEs in the chaotic cavity at wave number $k = 75.5\pi/d$: States associated with the direct transmission path are shown with their respective null-space and noiseless norms χ, σ . With increasing transverse quantization states have more overlap with the circular boundary part. For low-quality NOTEs diffraction effects are observed also here (see arrow in the bottom row).

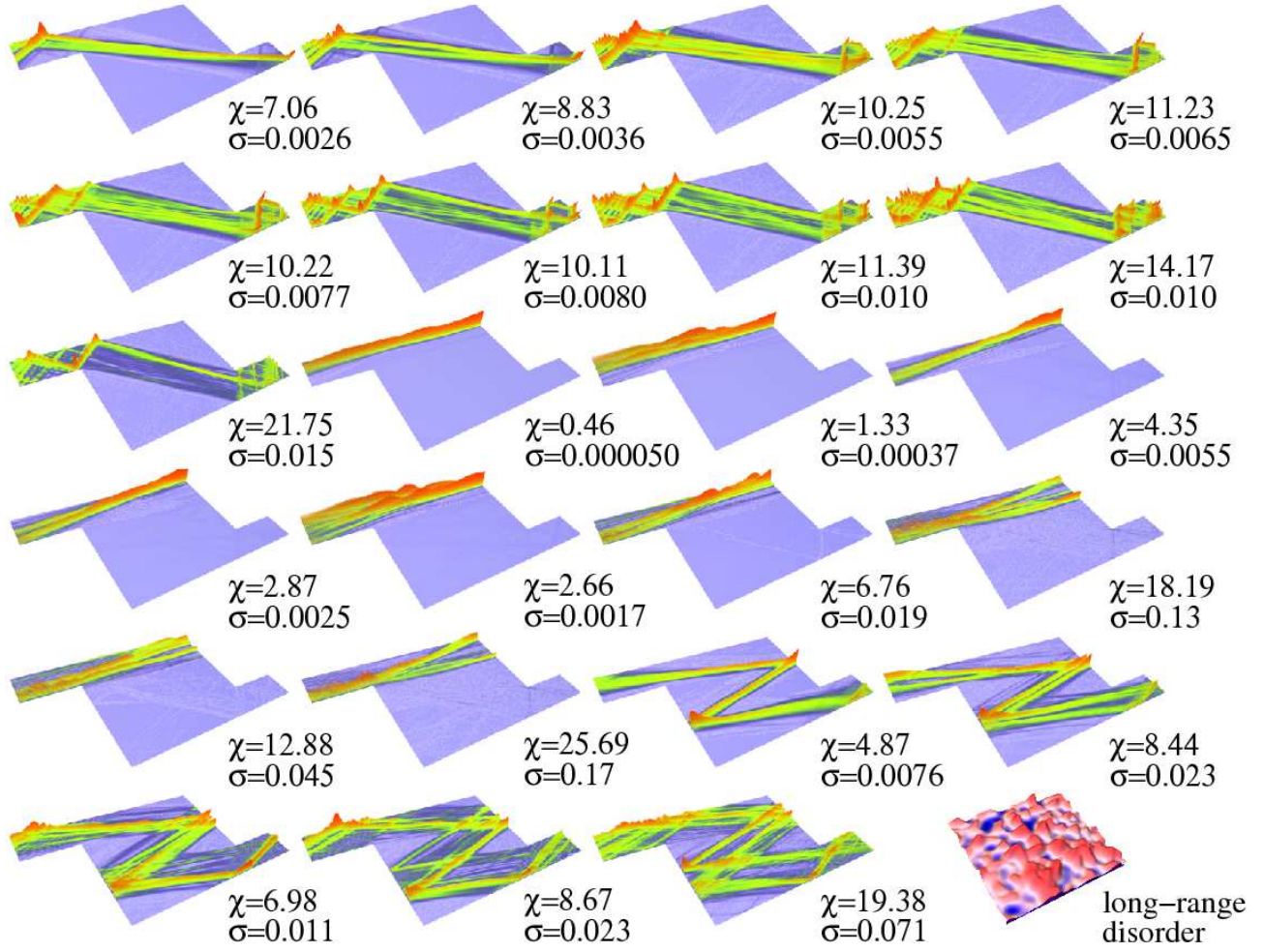


Fig. E.7: Wave function densities of NOTEs in the disordered cavity with long-range disorder at wave number $k = 75.5\pi/d$: all NOTEs with a null-space norm $\chi \lesssim 30$ are shown in the order of their time-delay value q_i . The number of states with this quality is here much larger than in the case of short-range disorder with the same disorder amplitude, $V_0 = 10\%E$ (see Fig. E.8 for comparison). The employed potential landscape with disorder correlation length $kr_c = 30\pi$ is shown in the rightmost panel in the bottom row.

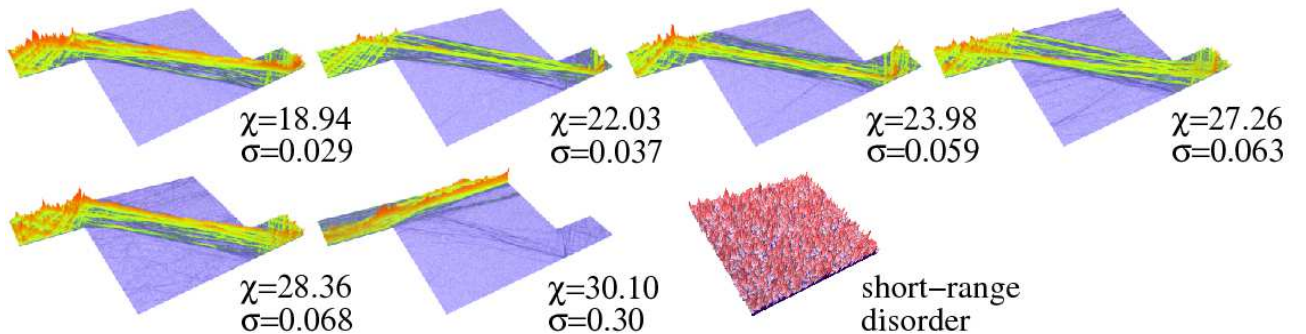


Fig. E.8: Wave function densities of NOTEs in the disordered cavity with short-range disorder at wave number $k = 75.5\pi/d$: all NOTEs with a null-space norm $\chi \lesssim 30$ are shown in the order of their time-delay value q_i . The disorder amplitude ($V_0 = 10\%E$) is here the same as in Fig. E.7, but the number of states with quality $\chi \lesssim 30$ is strongly reduced as compared to the case of long-range disorder. The employed potential landscape with disorder correlation length $kr_c = 5\pi$ is shown in the rightmost panel in the bottom row.